Experimental characterization and numerical modeling of damage at the mesoscopic scale of woven polymer matrix composites under quasi-static tensile loading

A. Doitrand, C. Fagiano, V. Chiaruttini, F.H. Leroy, A. Mavel, M. Hirsekorn

Experimental characterization and numerical modeling of damage at the mesoscopic scale of woven polymer matrix composites under quasi-static tensile loading

A. Doitrand, C. Fagiano, V. Chiaruttini, FH. Leroy, A. Mavel, M. Hirsekorn

Corresponding author: aurelien.doitrand@onera.fr - Tel: +33(0)146734658
ONERA - The French Aerospace Lab - F-92322 Châtillon - France

Abstract

The mechanical behavior of a four-layer plain weave glass fiber/epoxy matrix composite is modeled at the mesoscopic scale, taking into account the dry fabric preforming before resin injection, the relative shift and nesting between fabric layers, and the characteristic damage mechanisms, *i.e.*, intra-yarn cracking and decohesion at the crack tips. The surface strain fields obtained numerically are similar to the strain fields observed at the surface of the specimen. Damage is modeled by introducing discrete cracks in the FE mesh of the representative unit cell of the composite. The crack locations are determined using a stress based failure criterion. The predicted locations are similar to those observed experimentally. The effects of intra-yarn cracks on the macroscopic mechanical properties show the same trends as the experimental data. Good quantitative agreement is obtained if yarn/yarn or yarn/matrix decohesions at the crack tips are taken into account.

Keywords: Textile composites, Damage mechanics, Finite element analysis, Multiscale modeling, Transverse cracking

1. Introduction

Composite materials containing textile reinforcements are receiving a growing interest in advanced structural applications. One of the advantages of textile composites is the drapability of the reinforcing fabric, whose architecture can be varied throughout the

structure. In addition, complex reinforcement shapes may be directly woven with modern looms [1], which reduces the number of parts required for a composite structure, thus limiting the use of joints, which constitute classical weak points in the structure, and reducing the manufacturing costs.

In order to optimize the potential of woven composites and the mechanical performances of the resulting structures, design tools able to describe the evolution of the mechanical behavior from damage onset to final failure of the material are required. In recent years, macroscopic phenomenological models that successfully predict damage evolution and failure in textile composites have been developed for 2D [2, 3] and 3D [4, 5, 6] textile composites. However, the experimental identification of the model parameters is usually both expensive and time consuming. Moreover, the model parameters have to be identified experimentally each time the reinforcement architecture or the constituents change. Virtual material testing is a possible strategy for replacing some of the experimental tests during the design phase. For that purpose, predictive models based on a more physical description of damage are necessary. These models have to correlate the different characteristic scales of the material. Three different scales are identified for this kind of material. The microscopic scale is the scale of the constituents (fiber and matrix). At the mesoscopic scale, the reinforcement architecture is described by interlaced homogeneous fiber yarns embedded in the matrix. The macroscopic scale is the scale of the structure, at which the material is considered to be homogeneous. In order to set up predictive macroscopic damage models taking into account the reinforcement architecture, accurate damage modeling at the mesoscopic scale is required.

The reinforcement architecture of the textile composites is approximatively periodic. The weaving process, the handling of the fabric and the injection process during composite manufacturing induce small variations into the periodic structure of the yarn path and in the shapes of the yarn sections. Olave *et al.* [7] have shown that the mechan-

ical properties of the composite are not significantly influenced by these variations. In order to reduce computational costs, perfect periodicity is often assumed [8] by choosing a meso-scale smallest pattern representative of the whole material, called the representative unit cell (RUC). In order to obtain reliable results in terms of strain and stress field distributions, it is essential that the yarn shapes and their relative positions are close to those observed experimentally [8, 9]. Several tools have been proposed in the literature for the generation of textile geometrical models [10, 11, 12, 13]. However, most of them simplify the yarn shapes, generating possible interpenetrations between yarns and resulting in yarn volume fractions lower than those observed experimentally. In order to precisely model the characteristic damage mechanisms, the complex architecture of the material (*e.g.* nesting between layers, varying yarn shapes) must be taken into account in the geometrical model. Geometries close to the real architecture of the material can be obtained by simulating the preforming step of the dry fabric before resin injection [14, 15, 16].

At the mesoscopic RUC scale, damage can be modeled using different methods. An analytical model using a damaged mosaic laminate model has been proposed by Gao *et al.* [17]. It allows the calculation of the effective Young's modulus of the damaged composite, including three different damage modes. However, the use of a mosaic laminate does not take into account the yarn undulation which has a significant influence on the damage location, as shown by Melro *et al.* [18] and Daggumati *et al.* [19]. Most of the published studies use numerical approaches based on Finite Element (FE) analyses, which are more flexible since there are no limitations from a geometrical point of view. In the literature, different approaches have been proposed to generate FE meshes of woven composites RUC. A method that is widely used, due to its simplicity of implementation, is voxel meshing [9, 20, 21, 22]. This method is well suited to the prediction of the elastic properties of undamaged materials, but presents several limitations when attaining the damage onset

prediction [20]. Indeed, the yarn surfaces are not correctly represented by the element faces. The generation of consistent FE meshes with element faces that follow accurately the yarn surfaces is complex [14], especially in zones where yarns are in contact. Therefore, many authors insert a matrix layer between the yarns [8, 18, 23, 24], which considerably simplifies the meshing procedure since each yarn can be meshed separately. If the layer is thick, a lower yarn volume fraction is obtained in the RUC, and if it is thin, very small elements are required to ensure a good mesh quality. Therefore, the method of Grail *et al.* [14], which allows the generation of consistent meshes of 2D textile composite RUC with yarns in contact, will be used in this work. This method seems to be appropriate to model meso-scale damage in textile composites [20].

Most articles dealing with meso-scale damage modeling use continuum damage mechanics (CDM) with damage variables for matrix and yarns [18, 19, 25, 26, 27]. This method consists in detecting damage onset using a stress failure criterion, and then reducing the local stiffness of damaged elements with increasing loading. Models based on CDM allow studying the evolution of the mechanical properties with increasing damage, but can erroneously predict the direction of damage propagation [8, 26]. An approach that is closer to experimental observations of damage at the meso-scale is to describe damage through discrete cracks, which are inserted into the FE mesh after adapting this mesh locally in order to follow the crack path.

There are only few publications concerning discrete damage modeling in woven composites. Le Page *et al.* [28] have investigated the effects of a discrete crack on the strain energy release rate for a four-layered plain weave composite with different shifts between the layers (in-phase, out-of phase and random). The main limitation of this approach is the use of a simplified bi-dimensional geometrical model that does not take into account the complex 3D reinforcement architecture. Nevertheless, it has been shown that the energy release rate associated with an intra-yarn crack is influenced by the layer shifts.

Couegnat [10] has developed a tool able to insert cracks in 3D FE meshes of woven composites. A crack is represented by a plane and an idealized geometry of the fabric is used, including a matrix layer between yarns in order to make the meshing step easier. Therefore, the multiple and complex contact zones between yarns are not taken into account in the model. Recently, Obert *et al.* [29] have investigated the effects of mesoscopic damage by inserting discrete cracks in the yarns of a single ply of a 5H satin surrounded by homogenized plies with the aim of developing a model with damage variables related to the crack density in the yarns. This model does not take into account the interaction between the yarns of different layers. However, it has been shown in different studies that nesting between the layers of a multi-layered textile composite has to be taken into account since it can lead to different damage initiation scenarios, and different patterns of damage progression [24, 28].

The aim of this work is to model the characteristic damage mechanisms encountered at the mesoscopic scale and to evaluate their effects on the macroscopic mechanical behavior of the material. A detailed description of damage is proposed combining: *(i)* a realistic description of the meso-scale geometry obtained by modeling the preforming step of the dry fabric, *(ii)* a consistent mesh of the RUC, and *(iii)* discrete damage modeling. The influence of geometrical parameters on the effects of the characteristic damage mechanisms is evaluated. The procedure is illustrated on a RUC of a compacted and nested four-layered plain weave glass fiber/epoxy matrix composite. Several multi-instrumented experimental tests have been performed in order to characterize the damage mechanisms (sequence, locations) and evaluate their effects on the macroscopic mechanical behavior of the material. The experimental tests are presented in section 2. Then, the numerical procedure is presented including the generation and meshing of a compacted and nested RUC (section 3) and discrete damage modeling (section 4). In section 5, the results obtained numerically are compared with the experimental data in terms of: *(i)* surface

strain fields, *(ii)* detection of the damage locations and *(iii)* effects of mesoscopic damage on the macroscopic mechanical properties of the composite.

2. Experimental analysis

The composite under investigation consists of four layers of a plain weave reinforcement of E-glass fibers embedded in Araldite LY564 epoxy resin. The dry fabric was placed into a steel mold. By tightening the screws that keep the mold closed, the fabric is compacted, which increases the fiber volume fraction in the final composite and hence its mechanical properties. The amount of compaction is determined by measuring the thickness of the composite plate. Several specimens have been tested in order to characterize the meso-scale damage and its effects on the mechanical behavior of the material. First, two monotonic tensile tests were performed in order to determine: *(i)* the elastic properties of the material, *(ii)* the surface strain fields using Digital Image Correlation (DIC), *(iii)* the damage onset using Acoustic Emission (AE) and *(iv)* the failure stress. Then, an incremental tensile test was performed to analyze both damage location and kinetics using microscope observations on the edge of the specimen, as well as the evolution of the mechanical properties (Young's modulus, Poisson's ratio) of the material with increasing damage. The stress-strain curves of the tested specimens are shown in Figure 1.

2.1. Acoustic emission

The stress level associated with damage onset and failure of the material was determined using AE (Figure 1), as in references [30, 31]. The damage mechanisms result in a spontaneous release of elastic strain energy that is dissipated as a wave propagating through the material. Two sensors attached at the ends of the specimen (Figure 2a) detect these acoustic events, which can be related to a stress level.

2.2. Microscope observations

The location and the sequence of damage were determined using an optical microscope, as, for instance, in [32, 33]. Microscope observations on the specimen edge were performed at each loading step of the incremental tests. The observed damage mechanisms are: *(i)* intra-yarn cracks in the yarns that are transverse to the loading direction, *(ii)* debonding at the interface between cracked yarns and overlapping yarns or matrix and *(iii)* fiber failure in yarns, which leads to the composite failure (Figure 2b).

2.3. Digital image correlation

The differences between the mechanical behavior of the stiff fibers and of the compliant matrix result in heterogeneous strain fields with strong strain gradients, especially around yarn crimp regions. Classical electrical resistance strain gages can thus not provide an adequate spatial resolution. Therefore, the local strains on the composite surface have been measured using DIC, as in [34, 35]. The average strain is used to evaluate the loss of in-plane elastic properties of the material with increasing damage. The specimen stiffness E was estimated by a non-linear regression on stress/strain curves obtained by DIC (Equation 1).

$$\hat{\epsilon} = \epsilon_0 + \frac{1}{E}\sigma + a(< \sigma - \sigma_y >_+)^2 \tag{1}$$

where $<>_+$ are the Macaulay brackets (positive part). $\hat{\epsilon}$ is the estimated strain, ϵ_0 the strain offset at zero stress and σ the specimen stress. The quadratic part with the non-linearity coefficient, a, accounts for small non-linearities above the stress threshold, σ_y. Stresses significantly higher than σ_y, where the non-linearity becomes effective, are excluded from the regression. This quadratic part is added to take into account the uncertainty in the linearity limit σ_y. The resulting measurement uncertainty on E was evaluated by using a bootstrap procedure adapted to non-linear regression [36]. It should be noted that confidence intervals are dissymmetrical which results from the restriction of the σ_y threshold to a positive value, whose uncertainty is only left-bounded.

3. Finite element modeling of a Representative Unit Cell

3.1. Dry fabric compaction modeling

The use of a geometrical model of the reinforcement architecture that is as close as possible to that of the real specimen is essential in order to obtain an accurate meso-scale modeling [8, 9]. In order to increase the composite fiber volume fraction and thus to improve its mechanical performances, the dry preform is usually compacted before adding the matrix. The compaction phase has a significant influence on the yarn shapes and paths and must therefore be taken into account in a mesoscopic RUC. Indeed, complex yarn shapes can be generated during the manufacturing process, including: *(i)* local variations of both the section and the fiber volume fraction in the yarns [7, 37], *(ii)* random shifts and nesting between the layers [7, 38, 39], and *(iii)* complex contact regions between the yarns. The shape and the relative position of the yarns have a marked influence on the local strain and stress distributions in the composite, as well as on damage initiation and propagation [19, 28, 40]. Therefore, realistic geometries are required for accurate damage modeling at the mesoscopic scale.

Several automated tools have been proposed throughout the last decade to generate geometrical models of fabric reinforcements, and covering a large variety of weaving patterns [10, 11, 12, 13]. However, the deformation occurring during preforming is often neglected. Therefore, an idealized geometrical model of the fabric is commonly adopted, resulting in resin rich areas that are larger than those observed experimentally. As a consequence, in order to preserve the overall fiber volume fraction in the composite (typically between 50 and 60%), the fiber volume fraction in the yarns must be set to higher values than those observed in reality (sometimes 90%, or higher [41]). Yarn shapes closer to those of the real composite can be obtained from FE modeling of the dry fabric preforming [15, 16, 42]. In this work, the dry fabric compaction is simulated in order to generate geometries of a slightly unbalanced four-layered plain weave fabric. The advan-

tage of a plain weave fabric is that it has a relatively simple geometry with a small RUC. Nevertheless, due to compaction and nesting, multiple contacts zones between yarns are observed, which are significantly deformed with respect to their initial shapes. The initial geometry was generated using the 'TexGen' software [12], by imposing a relative shift between the layers that corresponds to the shifts observed experimentally on the edge of one of the tested specimens (Table 1). Then, the preforming step was simulated using Abaqus Standard (Figure 3) with the aim of obtaining: *(i)* a realistic yarn volume fraction, *(ii)* a qualitative reproduction of nesting between the layers and *(iii)* the deformation of the yarn cross section due to the neighboring yarns in contact. Since the final thickness of the reinforcement after compaction is imposed by the mold, the calculation of the exact force balance is not necessary. Moreover, the yarns are mainly deformed in transverse compression. Therefore, a transverse isotropic elastic behavior for the yarns is sufficient to obtain yarn shapes and positions close to those observed experimentally on the edge of the specimen (see Figure 4). Lin *et al.* [15] also showed that the most effective phenomena under compression are already well captured using such a simplfied behavior. The tensile modulus in the fiber direction (index L), $E_L = 40.92$GPa, has been determined according to the rule of mixtures for a fiber volume fraction of 55.6% in the yarns. The transverse (index T) and shear moduli have been arbitrarily fixed to a much smaller value ($E_T = G_{LT} = 4.1\ 10^{-3}$GPa) in order to ensure that the main deformation modes are bending and deformation of the transverse yarn section. The Poisson's ratio in the direction of the fibers ν_{LT} is zero, which means that transverse compaction of the yarn does not cause a change in its length. In order to ensure an approximately constant fiber volume fraction in the yarn, the transverse Poisson's ratio, ν_{TT}=1, should be used. However, too high a value of ν_{TT} leads to numerical instabilities and convergence issues; therefore, a lower value was chosen (ν_{TT}=0.7), resulting in yarn shapes similar to those observed experimentally. The normal contact behavior between the yarns was modeled

using hard contact, and the tangential behavior using a penalty method with a friction coefficient of 0.24 [43].

3.2. Consistent meshing of the Representative Unit Cell

In order to perform FE analysis, it is necessary to generate a mesh of the composite RUC, *i.e.*, the deformed reinforcement and the matrix complement. A consistent mesh of the RUC (Figure 5) is obtained using the procedure developed by Grail *et al.* [14]. This procedure ensures conformal meshes at the contact zones between the yarns and between yarns and matrix. Consequently, in the undamaged RUC the yarns are perfectly glued to each other and to the matrix, since common nodes are used in the contact zones. The FE mesh consists of quadratic tetrahedral elements in order to ensure an accurate modeling of the stress gradients. The mesh is then used to obtain the homogenized macroscopic elastic properties of the material using the method described in [20]. Periodic boundary conditions, as described in [8], are applied in the fabric plane directions of the RUC, whereas the top and bottom surfaces are left free in order to correctly represent the boundary conditions applied to the composite specimen subjected to a tensile test.

The matrix behavior is supposed to be linear elastic, and the mechanical properties provided by the manufacturer are: Young's modulus $E_m = 3.2$ GPa and Poisson's ratio $\nu_m = 0.35$. The yarn behavior is obtained by micro-meso homogenization, as in [18], using $E_f = 73.6$ GPa [44] and $\nu_f = 0.3$ for the fibers. The fiber volume fraction in the yarns is chosen in order to obtain an overall fiber volume fraction in the RUC similar to the fiber volume fraction in the real composite. The overall fiber volume fraction in the composite is calculated as a function of the number of fabric layers n_{layers}, the fabric mass per unit area σ_s, the mass density of the fibers ρ_{fiber} and the thickness of the specimen h (Equation 2).

$$V_f = \frac{n_{layers} * \sigma_s}{\rho_{fiber} * h} \tag{2}$$

The fabric properties given by the manufacturer are $\sigma_s = 504 \pm 40$ g.m^{-2} and $\rho_{fiber} = 2.54$

g.cm^{-3}. The thickness of the specimen is between 1.672 mm and 1.695 mm, with a mean value of $h = 1.679$ mm. The uncertainties of these fabric properties lead to a resulting fiber volume fraction in the composite between 43.1% and 51.3%. The overall fiber volume fraction in the RUC is chosen equal to $V_f = 49.2$ % in order to obtain a Young's modulus of the undamaged RUC that is close to the experimental Young's modulus of the undamaged specimen. This leads to a fiber volume fraction in the yarns of 55.6 %. A transverse isotropic elastic behavior is obtained for the yarns, with $E_l = 42.2$ GPa, $E_t = 9.93$ GPa, $\nu_{tt} = 0.423$, $\nu_{lt} = 0.319$ and $G_{lt} = 7.31$ GPa, where the index l refers to the fiber direction and the index t to the transverse direction. The local orientation of the yarn material is calculated separately at each integration point through orthogonal projection of its position on the neutral line of the yarn. The tangent to the neutral line at the projected point defines the axis of transverse isotropy of the yarn material (the fiber direction) at the integration point.

4. Discrete damage modeling

Damage in the form of discrete cracks is inserted into the RUC mesh in order to model its effects on the macroscopic mechanical behavior of the composite. The studied damage scenarios are based on experimental observations (section 2). In order to insert the cracks, some tools, initially developed by Chiaruttini *et al.* [45] for crack propagation simulation in metallic structures, are used.

The crack surface is inserted into the RUC mesh using a mesh intersection algorithm. Another possible method would be to generate the cracked mesh by using general Boolean operations on both meshes. However, Boolean operations between complex meshes are difficult to handle correctly using standard double precision encoding of the nodal positions. Indeed, numerous round-off errors make it impossible to obtain, in a robust way, a surface mesh that could be filled with tetrahedral elements using an automatic mesh generator. The algorithm used in this work allows the generation of an approximation

of the mesh that would have been built using a general Boolean operation between the volume mesh and a crack surface mesh, as detailed in [45].

Experimental observations show that, at the mesoscopic scale, the first damage is cracking in the yarns that are transversely oriented to the loading direction. At the same time, inter-yarn decohesions are observed at the crack tips. On the other hand, isolated decohesions, not related to transverse yarn cracks, are not observed in this material. This leads to the conclusion that damage onset is driven by transverse yarn cracking and that the decohesions between yarns or between yarn and matrix are a consequence of the transverse yarn cracks. The algorithm described previously is used to model these two damage mechanisms within the RUC. In most publications, the damage location is determined by a stress failure criterion [18, 19, 25]. For instance, Daggumati *et al.* [19] have shown that for a multi-layered 5-harness satin weave, damage onset occurs at the center of the yarn crimp zones for an outer layer, and at the edges of the yarn crimp zones for an inner layer. However, an idealized geometry of the yarns was used without shifts between the layers; therefore, the multiple and complex contact zones between yarns existing in real multi-layered composites were not taken into account. Experimentally, the location of cracks in yarns seems to be influenced by the local relative position of yarns [32].

In this work, a failure criterion developed for unidirectional plies is used in order to determine crack locations in the yarn [46], and a failure criterion for quasi-brittle materials is used for the matrix [47]. These criteria have already been used in a previous study in order to determine the damage onset mechanism and location in woven composites [20]. Since decohesions are a direct consequence of transverse yarn cracking in the studied material, a separate criterion for the onset of decohesions has not been used. Under different kinds of loading, the damage mechanisms may change, and in this case, the inserted type of damage has to be adapted. For instance, if decohesion was the first main

damage mechanism, a failure criterion able to predict decohesion onset would have to be used to determine the damage location. The equations and the damage mechanisms taken into account are summarized in Table 2. X_t and X_c are the tensile and compressive ply strengths in the direction of the fibers. Y_t and Y_c are the transverse tensile and compressive strengths. S_{12}^f and S_{13}^f are called the effective shear strengths. They are higher than the real shear strengths S_{12}^R and S_{13}^R of the ply such that damage onset is predicted correctly in a matrix-dominated mode (2 or 3) for pure shear loading, instead of the compressive fiber failure mode [48]. p_{12}, p_{13} and p_{23} are shape parameters that take into account the coupling between compressive and shear stresses. These parameters can be directly determined from the transverse compressive ply strength Y_c [48]. The values of the different parameters taken from Soden *et al.* [49], Charrier [48] and Laurin [50] are summarized in Table 3.

Several hypotheses are made concerning the geometry of the crack. The first assumption is that the crack, once nucleated, is supposed to propagate instantaneously across the whole yarn. Obert *et al.* [29] justified this assumption by arguing that the energy density is nearly uniform along a yarn. The second assumption is that the decohesion length is supposed to be constant and symmetric on each side of the crack which is inserted perpendicularly to the macroscopic loading direction.

The first step in the crack insertion process consists in determining the location of the first cracks in the undamaged RUC using the failure criterion described above, as shown in Figure 6 where $f = max(f_1^+, f_1^-, f_2^+, f_2^-, f_3^+, f_3^-, f_{matrix})$. At these locations, cracks are inserted into the FE mesh (Figure 6c). Then, a calculation with the damaged RUC leads to the determination of the location of new cracks (Figure 6d) that are also inserted into the RUC mesh. This process is repeated until the crack density in the RUC is close to the crack density measured experimentally on the specimen edge just before failure ($\rho_s = 0.87$ cracks/mm^2). In the undamaged zones of the material, the stress fields are

regular, thus providing a good estimation of possible locations of crack onset. However, stress concentrations are observed around the decohesion tips (or the crack tips if there is no decohesion) due to the geometric singularity (Figure 7). Therefore, the integration points in the immediate vicinity of decohesion or crack tips are not considered as possible locations of new cracks, even if the failure criterion is reached there first. The study of decohesion propagation would require an energy based fracture mechanics approach, which constitutes the subject of ongoing activities.

5. Comparison between numerical and experimental results

The numerical and experimental surface strain distributions are similar (Figure 8a and b). This result may be attributed to the fact that the relative layer positions in the RUC were determined experimentally from microscope observations on the edge of the specimen. In order to obtain a quantitative comparison between both methods, the FE results were smoothed on a zone corresponding to the DIC resolution window. Along a line (Figure 8a and b), the numerical and experimental transverse strains are close to each other (Figure 8c).

The final damaged RUC (with a crack density close to that measured experimentally just before failure) obtained using the procedure presented in section 4 contains 14 cracks and is shown in Figure 9. The crack locations obtained with the FE model are compared to several microscope observations (corresponding to a RUC length) on the edge of the same specimen (Figure 10). It can be seen that some cracks appear at similar locations in the RUC over the whole specimen length, showing a certain regularity of damage in the material. In addition, some variability is detected within the zones with repeating damage patterns, both in terms of crack position and number. Furthermore, several crack locations are observed only once. Both phenomena result from the material having an overall periodic architecture, with local variations due to: *(i)* dry fabric preforming, *(ii)* matrix injection, *(iii)* possible defects inside the material, etc. Despite the fact that

edge effects are not taken into account in the model, the numerical and experimental crack locations are quite similar. Therefore, it seems to be reasonable to assume that the overall influence of the edge effects on the crack location is, in this case, relatively weak. However, these effects may partially be responsible for the differences between numerical predictions and experimental observations. Other possible causes that may explain these differences could be the crack modeling hypotheses and the material variability that is not taken into account.

The decrease in Young's modulus (E_{11}) and in Poisson's ratio (ν_{12}) with growing crack density (ρ_s) is compared to experimental data for different decohesion lengths (μ) (Figure 11). The crack density is the number of cracks per unit area on the specimen edge. The crack density used in the numerical simulations may not be exactly equal to the crack densities at which the elastic properties have been measured experimentally. Therefore, since the numerically calculated trends of the elastic properties are continuous, the results are interpolated (lines connecting the numerically calculated values in Figure 11) before comparing them to the experimental values. The evolution trends of Young's modulus and of Poisson's ratio are in good agreement with the experimental data. Moreover, it is necessary to take into account the decohesions at the crack tips, otherwise the reduction of the properties would be underestimated. For example, the maximum reduction of Young's modulus observed experimentally is 5.82 ± 1.16 % at a crack density of $\rho_s = 0.92$ cracks.mm^{-2}. Without decohesions at the crack tips, the numerical model only yields a reduction of 3.28 % at that value of ρ_s. A decohesion length of $\mu = 0.07$ mm gives a better approximation of the measured Young's moduli and Poisson's ratios as a function of crack density.

Microscope observations show that some intra-yarn transverse cracks are not exactly perpendicular to the loading direction, but slightly disoriented with a small tilt angle (Figure 2b). The reduction of the elastic properties as a function of the crack density

has been calculated for a RUC with cracks perpendicular to the loading direction and compared to a RUC with tilted cracks, with a tilt angle varying from $-40°$ to $40°$ with respect to the normal to the composite surface. The differences obtained between the RUCs with perpendicular and tilted cracks are below 0.5% for E_{11}, 1.3% for ν_{12} and 2.2% for G_{12}. Therefore, we conclude that the crack tilt only has a minor influence on the in-plane homogenized macroscopic properties.

6. Conclusion

A strategy for the numerical modeling of damage at the mesoscopic scale of woven polymer matrix composites has been presented. The complex geometry of the reinforcement in the RUC is correctly described by modeling the dry fabric preforming before resin injection. A consistent FE mesh of a four-layered plain weave fabric with shifts between layers determined from experimental observations is used to model the mechanical behavior of the woven composite. The surface strain fields obtained numerically are in good agreement with the strain fields observed at the surface of the specimen.

Damage is introduced into the FE model of the RUC by inserting discrete cracks including decohesions at the crack tips in yarns transverse to the loading direction. The prediction of the location of damage is computed using a stress failure criterion able to take into account different damage mechanisms in yarns and matrix. The crack locations obtained with the FE model are quite similar to experimental observations, even if some differences are observed. However, the stress criterion is only a necessary condition for a crack onset, but not a sufficient one, since crack onset is possible only if the energy release rate is also high enough. Therefore, a criterion based on both stress and energy will be used in future works. An energy-based error estimator will also be used to ensure the energetic convergence of the FE meshes.

The decrease in the homogenized in-plane macroscopic properties with damage growth is in good agreement with experimental data if decohesions at the crack tips are taken

into account. In this article, the decohesion length has been assumed to be the same around each crack tip and the influence of this average length on the macroscopic properties has been studied. Future work will consist in applying fracture mechanics based methods together with numerical tools for the simulation of crack propagation to estimate quantitatively the size and shape of the decohesion zones. The crack orientation only has a minor influence on the in-plane macroscopic properties, but its effect on the out-of-plane properties still needs to be further studied. Using microscope observations, damage can only be characterized on the edge of the composite material, and additional experimental characterization (using for instance thermography or micro-computed tomography ($\mu - CT$)) will be required to better understand the damage mechanisms inside the material and to validate the modeling hypotheses, in particular the crack length along the yarns and the size of the decohesion zones.

References

[1] Mouritz A, Bannister M, Falzon P, Leong K. Review of applications for advanced three-dimensional fibre textile composites. Compos Part A 1999;30:1444-61.

[2] Hochard C, Aubourg PA, Charles JP. Modelling of the mechanical behaviour of woven-fabric CFRP laminates up to failure. Compos Sci Technol 2001;61:221-30.

[3] Barbero EJ, Lonetti P, Sikkil KK. Finite element continuum damage modeling of plain weave reinforced composites. Compos Part B 2005;37(23):137-47.

[4] Maire JF, Chaboche JL. A new formulation of continuum damage mechanics (CDM) for composite materials. Aerospace Science and Technology 1997;1(4):247-57.

[5] Marcin L. Modélisation du comportement, de l'endommagement et de la rupture de composites à renforts tissés pour le dimensionnement robuste de structures. Ph.D. Thesis, Université de Bordeaux 1, 2010. http://www.onera.fr/fr/publications-scientifiques.

[6] Rakotoarisoa C, Laurin F, Hirsekorn M, Maire JF, Olivier L. Development of a fatigue model for 3D woven polymer matrix composites based on a damage model. In Proceedings of ECCM15, Venice, Italy, 2011, paper 101.

[7] Olave M, Vanaerschot A, Lomov S, Vandepitte D. Internal geometry variability of two woven composites and related variability of the stiffness. Polym Compos 2012;33(8):1335-50.

[8] Lomov SV, Ivanov DS, Verpoest I, Zako M, Kurashiki T, Nakai H, Hirosawa S. Meso-FE modelling of textile composites: Road map, data flow and algorithms. Compos Sci Technol 2007;67(9):1870-91.

[9] Green SD, Matveev MY, Long AC, Ivanov D, Hallett SR. Mechanical modelling of 3D woven composites considering realistic unit cell geometry. Compos Struct 2014;118:284-93.
[10] Couegnat G. Approche multiéchelle du comportement mécanique de matériaux composites à renfort tissé. Ph.D. thesis, Université de Bordeaux 1, 2008. https://tel.archives-ouvertes.fr/tel-00403885/
[11] Verpoest I, Lomov SV. Virtual textile composites software WiseTex: Integration with micro-mechanical, permeability and structural analysis. Compos Sci Technol 2005;65:2563-74.
[12] Sherburn M. Geometric and mechanical modelling of textiles. Ph.D. thesis, The University of Nottingham, 2007. http://eprints.nottingham.ac.uk/10303/
[13] Adanur S, Liao T. 3D modeling of textile composite preforms. Compos Part B 1998;29:787-93.
[14] Grail G, Hirsekorn M, Wendling A, Hivet G, Hambli R. Consistent Finite Element mesh generation for meso-scale modeling of textile composites with preformed and compacted reinforcements. Compos Part A 2013;55:143-51.
[15] Lin H, Sherburn M, Crookston J, Long A, Clifford M, Jones I. Finite element modelling of fabric compression. Model Simul Mater Sci Eng 2008;16(3)035010(16pp).
[16] Nguyen QT, Vidal-Sallé E, Boisse P, Park CH, Saouab A, Breard J, Hivet G. Mesoscopic scale analyses of textile composite reinforcement compaction. Compos Part B 2012;44(1):231-41.
[17] Gao XL, Li K, Mall S. A mechanics-of-materials model for predicting Young's modulus of damaged woven fabric composites involving three damage modes. Int J Solids Struct 2003;40:981-99.
[18] Melro P, Camanho P, Andrade Pires FM, Pinho ST. Numerical simulation of the non-linear deformation of 5-harness satin weaves. Comput Mater Sci 2012;61(0):116-26.
[19] Daggumati S, Van Paepegem W, Degrieck J, Xu J, Lomov SV, Verpoest I. Local damage in a 5-harness satin weave composite under static tension: Part II Meso-FE modelling. Compos Sci Technol 2010;70:1934-41.
[20] Doitrand A, Fagiano C, Irisarri FX, Hirsekorn M. Comparison between voxel and consistent meso-scale models of woven composites. Compos Part A 2015;73:143-54.
[21] Zeng X, Brown LP, Endruweit A, Matveev M, Long AC. Geometrical modelling of 3D woven reinforcements for polymer composites: Prediction of fabric permeability and composite mechanical properties. Compos Part A 2014;56:150-60.
[22] Potter E, Pinho ST, Robinson P, Iannucci L, McMillan AJ. Mesh generation and geometrical modeling of 3D woven composites with variable tow cross-sections. Comput Mater Sci 2012;51(1):103-11.
[23] Stig F, Hallström S. A modelling framework for composites containing 3D reinforcement. Compos Struct 2012;94(9):2895-901.
[24] De Carvalho NV, Pinho ST, Robinson P. Numerical modelling of woven composites: biaxial loading. Compos Part A 2012;43(8):1326-37.
[25] Zako M, Uetsuji Y, Kurashiki T. Finite element analysis of damaged woven fabric composite materials. Comp Sci Technol 2003;63:507-16.

[26] Gorbatikh L, Ivanov D, Lomov SV, Verpoest I. On modelling of damage evolution in textile composites on meso-level via property degradation approach. Compos Part A 2007;38:2433-42.
[27] Römelt P, Cunnigham PR. A multi-scale finite element approach for modelling damage progression in woven composite structures. Compos Struct 2012;94(3):977-86.
[28] Le Page BH, Guild FJ, Ogin SL, Smith PA. Finite element simulation of woven fabric composites. Compos Part A 2004;35:861-72.
[29] Obert E, Daghia F, Ladevèze P, Ballere L. Micro and meso modeling of woven composites: Transverse cracking kinetics and homogenization. Compos Struct 2014;117:212-21..
[30] Lomov SV, Ivanov DS, Truong TC, Verpoest I, Baudry F, Vanden Bosche K, Xie H. Experimental methodology of study of damage initiation and development in textile composites in uniaxial tensile test. Compos Sci Technol 2008;68:2340-49.
[31] Daggumati S, De Baere I, Van Paepegem W, Degrieck J, Xu J, Lomov SV, Verpoest I. Local damage in a 5-harness satin weave composite under static tension: Part I Experimental analysis. Compos Sci Technol 2010;70(13):1926-33.
[32] De Carvalho NV, Pinho ST, Robinson P. An experimental study of failure initiation and propagation in 2D woven composites under compression. Compos Sci Technol 2011;71:1316-25.
[33] Böhm R, Hufenbach W. Experimentally based strategy for damage analysis of textile-reinforced composites under static loading. Compos Sci Technol 2010;70:1330-7.
[34] Lomov SV, Ivanov DS, Verpoest I, Zako M, Kurashiki T, Nakai H, Molimard J, Vautrin A. Full-field strain measurements for validation of meso-FE analysis of textile composites. Compos Part A 2008;39(8):1218-31.
[35] Koohbor B, Ravindran S, Kidane A. Meso-scale strain localization and failure response of an orthotropic woven glass-fiber reinforced composite. Compos Part B 2015;78:308-18.
[36] Flachaire E. Les méthodes du bootstrap dans les modèles de régression. Economie et prévision 2000;142:183-194.
[37] Karahan M, Lomov SV, Bogdanovich AE, Mungalov D, Verpoest I. Internal geometry evaluation of non-crimp 3D orthogonal woven carbon fabric composite. Compos Part A 2010;41:1301-11.
[38] Chen B, Lang EJ, Chou TW. Experimental and theoretical studies of fabric compaction behavior in resin transfer molding. Mater Sci Eng 2001;317:188-96.
[39] Lomov SV, Verpoest I, Peeters T, Roose D, Zako M. Nesting in textile laminates: geometrical modelling of the laminate. Compos Sci Technol 2003;63:993-1007.
[40] John S, Herszberg I, Coman F. Longitudinal and transverse damage taxonomy in woven composite components. Compos Part B 2001;32(8):659-68.
[41] Ivanov DS, Baudry F, Van Den Broucke B, Lomov SV, Xie H, Verpoest I. Failure analysis of triaxial braided composite. Compos Sci Technol 2009;69(9):1372-80.
[42] Stig F, Hallström S. Spatial modelling of 3D-woven textiles. Compos Struct 2012;94(5):1495-502.
[43] Badel P. Analyse mésoscopique du comportement mécanique des renforts tissés de composites utilisant la tomographie aux rayons X. Ph.D. Thesis, INSA Lyon, 2008.

http://theses.insa-lyon.fr/publication/2008ISAL0085/these.pdf
[44] Rocher JE, Allaoui S, Hivet G, Gillibert J, Blond E. Experimental characterization and modeling of GF/PP commingled yarns tensile behavior. J Compos Mater, 2015;49(21):2609-24.
[45] Chiaruttini V, Riolo V, Feyel F. Advanced remeshing techniques for complex 3D crack propagation. 13^{th} International Conference on Fracture 2013, Beijing, China;1:547-55.
[46] Laurin F, Carrère N, Maire JF. A multiscale progressive failure approach for composite laminates based on thermodynamical viscoelastic and damage models. Compos Part A 2007;38(1):198-209.
[47] Chaboche JL, Lesne PM, Maire JF. Phenomenological damage mechanics of brittle materials with description of unilateral damage effects. US-Europe Workshop on Fracture and Damage in Quasibrittle Structures 1994, Prague, Czeck Rep, 75-84.
[48] Charrier JS. Développement de méthodologies dédiées à l'analyse robuste de la tenue de structures composites sous chargements complexes tridimensionnels. Ph.D. thesis, ENSAM Paris, 2013. http://www.onera.fr/fr/publications-scientifiques.
[49] Soden PD, Hinton MJ, Kaddour AS. Lamina properties, lay-up configurations and loading conditions for a range of fibre-reinforced composite laminates. Compos Sci Technol 1998;58:1011-22.
[50] Laurin F. Approche multiéchelle des mécanismes de ruine progressive des matériaux stratifiés et analyse de la tenue de structures composites. Ph.D. Thesis, University of Franche-Comté, 2005. http://www.onera.fr/fr/publications-scientifiques.

Figure captions

Fig. 1 - Stress-strain curves of the tested specimens and cumulated acoustic emission energies as a function of the specimen strains.

Fig. 2 - Optical microscope observation of the damage pattern on the specimen edge, just before failure: (a) experimental set-up and (b) damage pattern (the picture was not taken at the failure location).

Fig. 3 - FE simulation of the compaction of four layers of plain weave fabric: (a) before compaction and (b) after FE compaction (ϵ_{33} is the compaction strain).

Fig. 4 - Yarn shapes (a) observed experimentally on the specimen edge and (b) obtained numerically through dry fabric compaction modeling.

Fig. 5 - FE mesh of the compacted RUC where the shifts between the fabric layers are determined from microscope observations: (a) meshed RUC and (b) visualization of the meshed yarns in the RUC.

Fig. 6 - Schematic representation of the damage modeling algorithm: (a) failure criterion in the undamaged RUC, (b) crack locations predicted by the failure criterion, (c) insertion of cracks at the predicted locations, and (d) prediction of new cracks resulting from the failure criterion in the damaged RUC.

Fig. 7 - Failure criterion in a cracked yarn and zoom to the area around the crack tip.

Fig. 8 - Qualitative comparison between (a) computed (6 dashed line delimited RUCs) and (b) measured (DIC) transverse strain fields under tensile (blue arrows) loading (macroscopic strain $\epsilon_{yy} = 0.0036$). (c) quantitative comparison along the dotted lines.

Fig. 9 - Damaged RUC containing 14 longitudinal cracks in the transverse yarns and the corresponding decohesions at the crack tips on the yarn surfaces.

Fig. 10 - Comparison between the crack locations predicted using the failure criterion and experimental observations on the specimen edge: (a), (b), (c), (d), (e) experimental examinations in various areas (RUC size) on the specimen edge and (f) crack locations predicted through the failure criterion.

Fig. 11 - Comparison between experimental and numerical results of the effect of transverse cracks in the weft yarns on Young's modulus (a) and on Poisson's ratio (b) in the warp direction as a function of the crack density ρ_s and the decohesion length μ.

Shifts with respect to layer 1 (top layer)	Δx (mm) (Warp direction)	Δy (mm) (Weft direction)
Layer 2	-0.61	-0.30
Layer 3	-0.59	3.43
Layer 4 (bottom layer)	0.43	2.93

Table 1: Layer shifts in warp and weft directions with respect to the top layer (the layers are sorted in z coordinate decreasing order).

Fiber failure	$f_1^+ = (\frac{<\sigma_{11}>^+}{X_t})^2$ $f_1^- = (\frac{<-\sigma_{11}>^+}{X_c})^2 + (\frac{\tau_{12}}{S_{12}^f(1-p_{12}\sigma_{22})})^2 + (\frac{\tau_{13}}{S_{13}^f(1-p_{13}\sigma_{33})})^2$ $< x >^+ = x$ if $x > 0, < x >^+ = 0$ otherwise	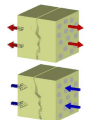
Transverse cracking	$f_2^+ = (\frac{<\sigma_{22}>^+}{Y_t})^2 + (\frac{\tau_{12}}{S_{12}^R(1-p_{12}\sigma_{22})})^2 + (\frac{\tau_{23}}{S_{23}^R(1-p_{23}(\sigma_{22}+\sigma_{33}))})^2$ $f_2^- = (\frac{<-\sigma_{22}>^+}{Y_c})^2 + (\frac{\tau_{12}}{S_{12}^R(1-p_{12}\sigma_{22})})^2 + (\frac{\tau_{23}}{S_{23}^R(1-p_{23}(\sigma_{22}+\sigma_{33}))})^2$	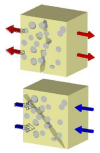
Out-of-plane cracking	$f_3^+ = (\frac{<\sigma_{33}>^+}{Y_t})^2 + (\frac{\tau_{13}}{S_{13}^R(1-p_{13}\sigma_{33})})^2 + (\frac{\tau_{23}}{S_{23}^R(1-p_{23}(\sigma_{22}+\sigma_{33}))})^2$ $f_3^- = (\frac{<-\sigma_{33}>^+}{Y_c})^2 + (\frac{\tau_{13}}{S_{13}^R(1-p_{13}\sigma_{33})})^2 + (\frac{\tau_{23}}{S_{23}^R(1-p_{23}(\sigma_{22}+\sigma_{33}))})^2$	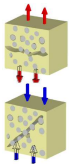
Matrix cracking	$f_{matrix} = \frac{((<\sigma_I>^+)^p + (<\sigma_{II}>^+)^p + (<\sigma_{III}>^+)^p)^{1/p}}{X}$	

Table 2: Failure criterion including different damage mechanisms such as fiber failure, transverse, and out-of-plane cracking for the yarns, and inter yarn matrix cracking for the matrix.

Strength	X_t	X_c	Y_t	Y_c	S_{12}^R	S_{13}^R	S_{23}^R	S_{12}^f	S_{13}^f	X
(MPa)	1140	570	35	114	72	72	45	83	83	80

Table 3: Values of the parameters of the failure criterion (Table 2).

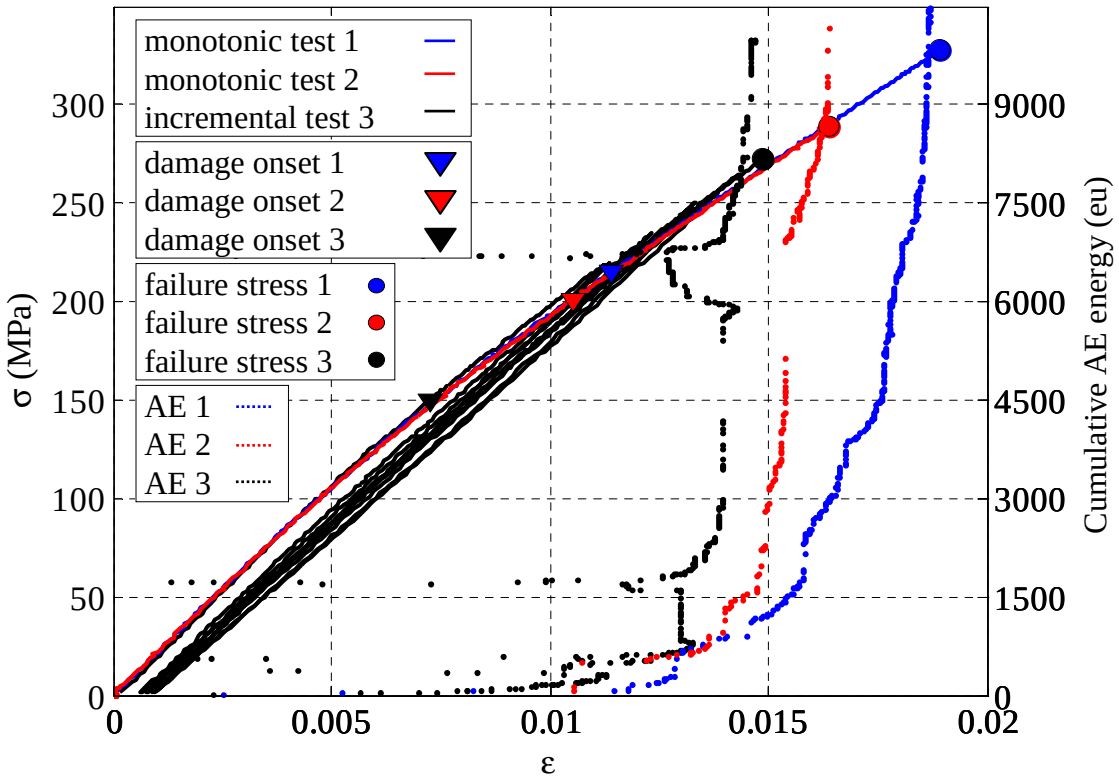

Figure 1:

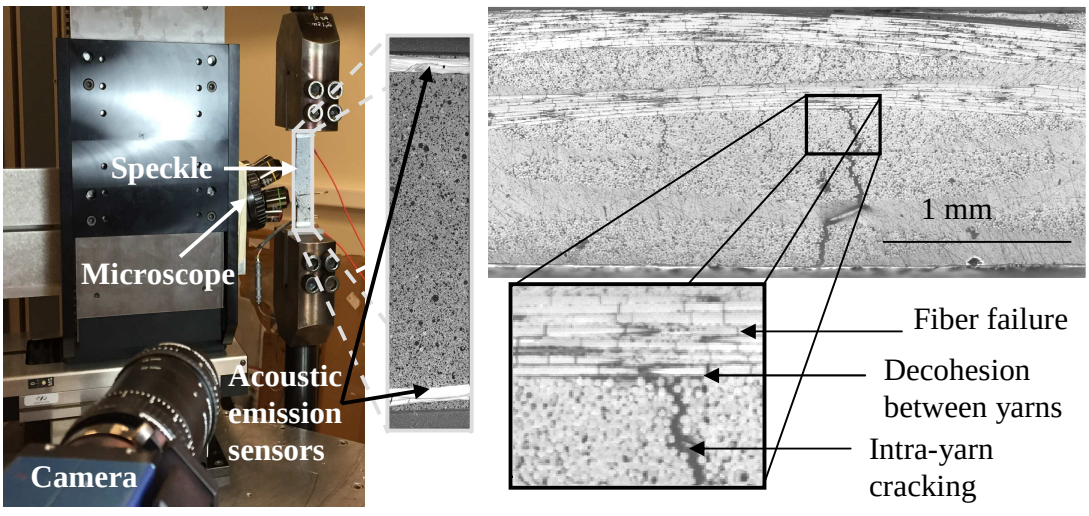

(a) (b)

Figure 2:

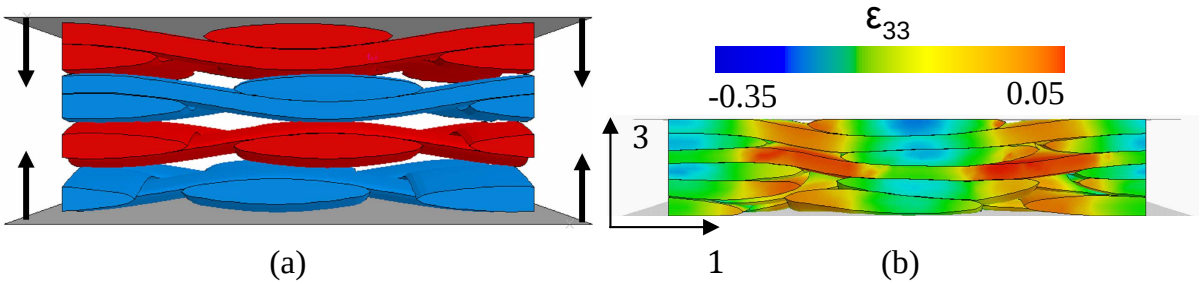

Figure 3:

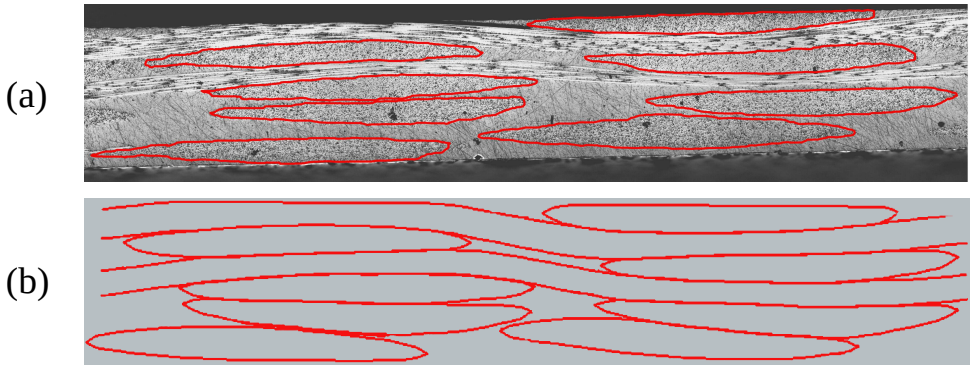

Figure 4:

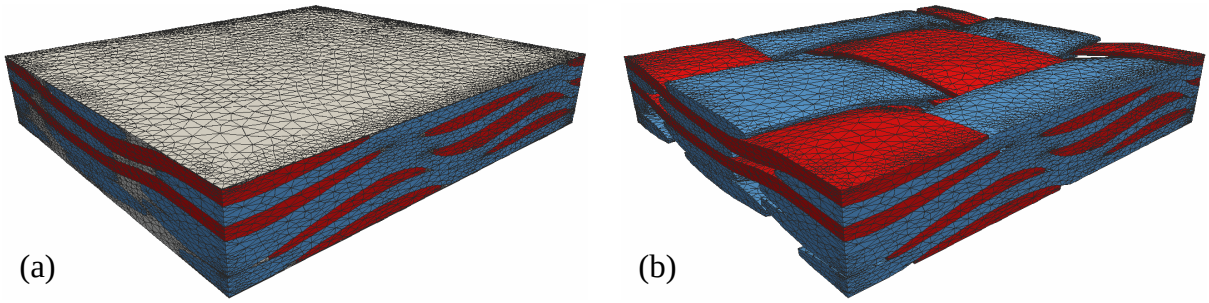

Figure 5:

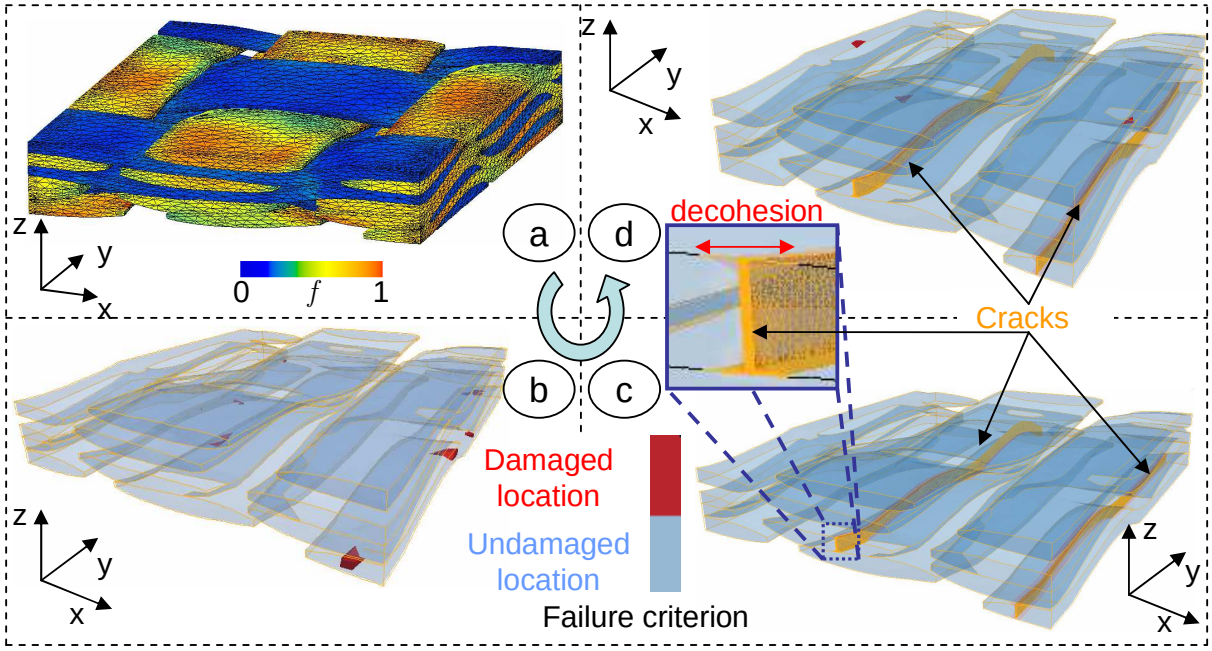

Figure 6:

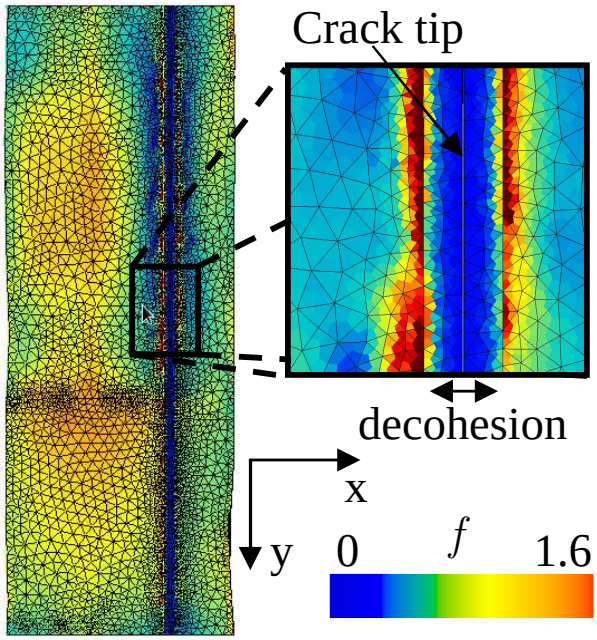

Figure 7:

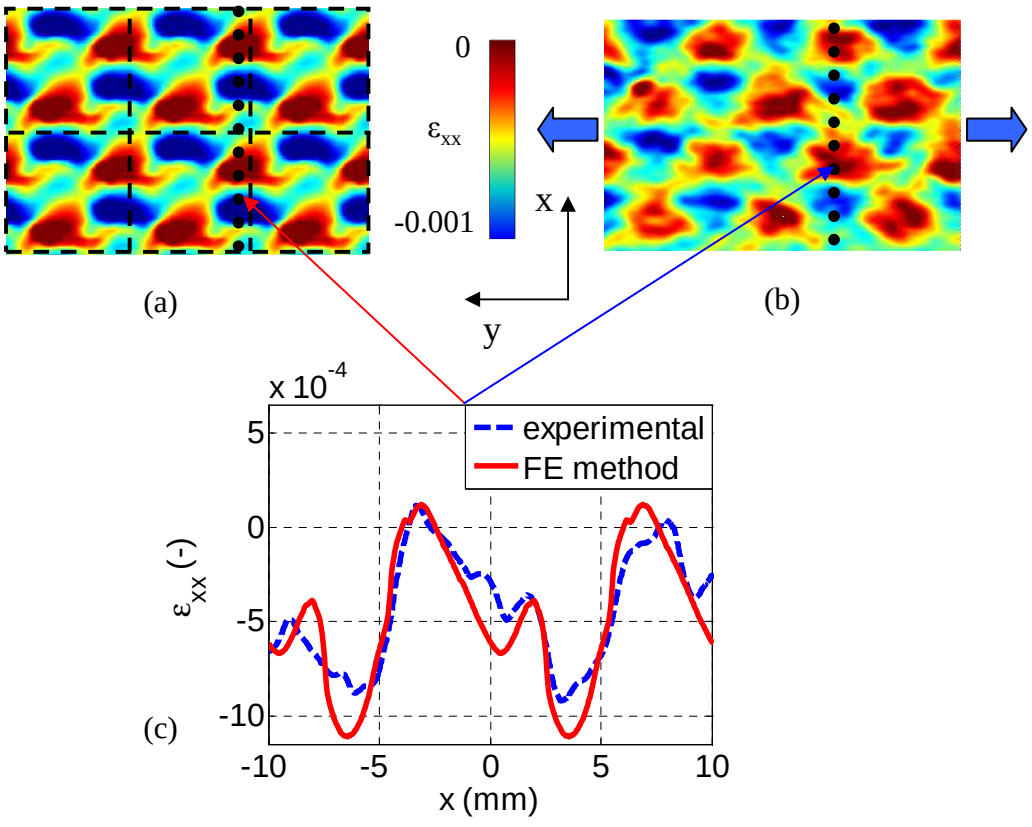

Figure 8:

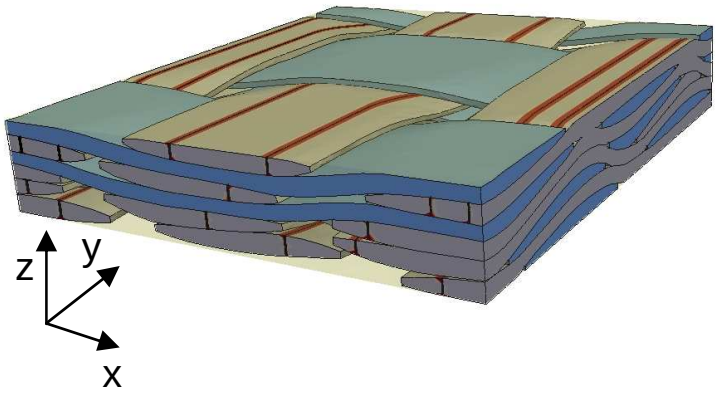

Figure 9:

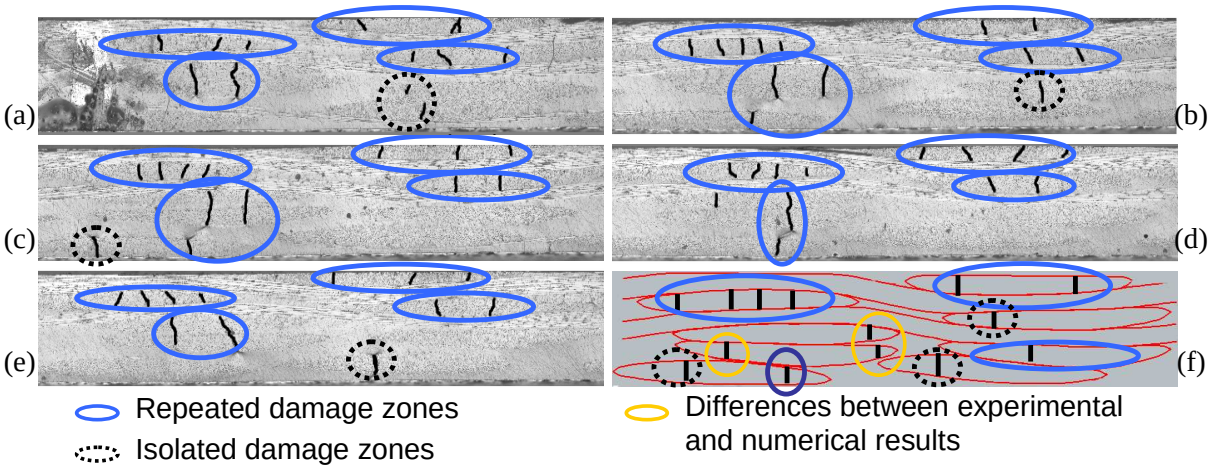

Figure 10:

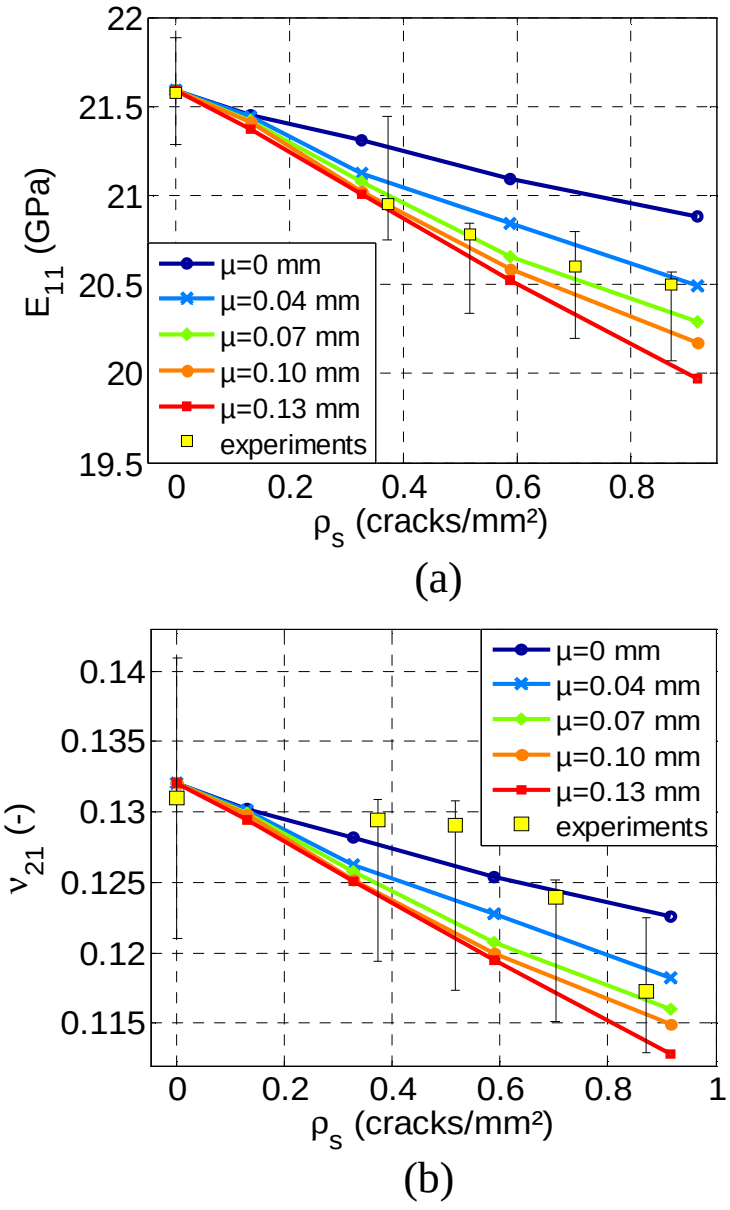
22
21.5
21
20.5
20
19.5
E11 (GPa)
0
0.2
0.4
0.6
0.8
ρs (cracks/mm²)
μ=0 mm
μ=0.04 mm
μ=0.07 mm
μ=0.10 mm
μ=0.13 mm
experiments
(a)
0.14
0.135
0.13
0.125
0.12
0.115
ν21 (-)
0
0.2
0.4
0.6
0.8
1
ρs (cracks/mm²)
μ=0 mm
μ=0.04 mm
μ=0.07 mm
μ=0.10 mm
μ=0.13 mm
experiments
(b)

Figure 11: